Research Square

Preprints are preliminary reports that have not undergone peer review.
They should not be considered conclusive, used to inform clinical practice,
or referenced by the media as validated information.

A Coupled Plasma-Assisted Growth and Electrochemical Modelling Framework for Predicting the Supercapacitor Performance of Vertically Oriented Graphene Nanosheets

Neha Jain

nehagpt2105@gmail.com

Maharaja Agrasen Institute of Technology

Suresh C. Sharma

Delhi Technological University

Research Article

Keywords: Plasma-enhanced chemical vapor deposition, Vertically oriented graphene nanosheets, Supercapacitor, Electric double-layer capacitance, Pseudocapacitance

Posted Date: August 20th, 2026

DOI: https://doi.org/10.21203/rs.3.rs-10629514/v1

License: This work is licensed under a Creative Commons Attribution 4.0 International License.
Read Full License

Additional Declarations: No competing interests reported.

A Coupled Plasma-Assisted Growth and Electrochemical Modelling Framework for Predicting the Supercapacitor Performance of Vertically Oriented Graphene Nanosheets

Neha Jain[1] and Suresh C. Sharma[2]

[1] Department of Applied Sciences (Physics), Maharaja Agrasen Institute of Technology, Sector 22, Rohini, Delhi, India

[2] Department of Applied Physics, Delhi Technological University, Shahbad Daulatpur, Rohini, Delhi

Abstract

A coupled plasma-assisted growth and electrochemical modelling framework is developed to establish a quantitative relationship between plasma-enhanced chemical vapor deposition (PECVD) operating conditions, vertically oriented graphene nanosheet (VGNS) morphology, and supercapacitor performance. Plasma characteristics obtained from a two-dimensional axisymmetric COMSOL model are coupled with a reduced-order growth model to determine the evolution of nanosheet height, thickness, and electrochemically accessible surface area under different chamber pressures and RF powers. Plasma-induced defect generation and electrochemically active-site formation are further incorporated into the electrochemical model to evaluate the individual contributions of electric double-layer capacitance (EDLC) and pseudocapacitance. The results show that decreasing the chamber pressure and increasing the RF power promote the growth of taller VGNS with a larger electrochemically accessible surface area while simultaneously increasing the density of electrochemically active sites. Consequently, the projected capacitance increases under more energetic plasma conditions, with EDLC remaining the dominant charge-storage mechanism and pseudocapacitance providing an additional contribution through plasma-induced surface activation. The model predicts a maximum projected capacitance of 196 $\mu F\ cm^{-2}$, which is in good agreement with reported experimental values for plasma-grown VGNS electrodes. The proposed framework provides a physically consistent basis for understanding the coupled effects of plasma processing, graphene growth, and electrochemical behaviour, and offers a practical computational tool for optimizing PECVD conditions for VGNS-based supercapacitor electrodes.

Keywords: Plasma-enhanced chemical vapor deposition, Vertically oriented graphene nanosheets, Supercapacitor, Electric double-layer capacitance, Pseudocapacitance.

1. Introduction

There is an ever-increasing demand for efficient, sustainable, and high-performance energy storage technologies to meet the rapidly growing requirements of portable electronics, electric vehicles, smart grids, and renewable energy systems [1]. Among the available electrochemical energy storage devices, supercapacitors have emerged as promising candidates because of their high power density, rapid charge-discharge capability, excellent cycling stability, and superior operational safety [2,3]. Despite these advantages, their relatively low energy density continues to limit widespread commercial deployment [4]. Since the electrochemical performance of supercapacitors is primarily governed by the properties of the electrode material, considerable efforts have been devoted to developing nanostructured electrodes with high surface area, excellent electrical conductivity, and efficient ion transport characteristics [5]. These developments have positioned carbon-based nanomaterials as one of the most promising classes of electrode materials for next-generation supercapacitors[6-8].

Among them, graphene has emerged as one of the most extensively investigated carbon materials for supercapacitor electrodes because of its exceptional electrical conductivity [9], high theoretical specific surface area (~2630 $m^2 g^{-1}$) [10], excellent mechanical strength [11], and near-infrared optical transparency [12],. However, the electrochemical performance of planar graphene is often limited by irreversible sheet restacking during electrode fabrication [13], which reduces the accessible surface area and restricts electrolyte-ion transport [14]. To overcome these limitations, vertically oriented graphene nanosheets (VGNS) have attracted significant attention owing to their two-dimensional interconnected architecture. Unlike planar graphene, VGNS consist of vertically aligned nanosheets with exposed graphene edges and open ion transport channels, providing improved electrolyte accessibility, shorter ion diffusion pathways, and a larger electrochemically active surface. In addition to enhancing electric double-layer charge storage, the abundant edge defects and exposed active sites present in VGNS can contribute to pseudocapacitive charge storage, resulting in superior electrochemical performance compared with conventional graphene electrodes [8,15–19].

Among the various techniques available for the synthesis of VGNS, plasma-enhanced chemical vapor deposition (PECVD) has emerged as one of the most versatile approaches because it enables precise control over plasma density, electron temperature, ion energy, and the concentration of reactive species during growth [20,21]. Unlike conventional thermal CVD, PECVD provides an additional degree of control through plasma-assisted reactions, allowing graphene nucleation, vertical growth, defect formation, and surface activation to be tailored by adjusting the plasma operating conditions. Consequently, processing parameters such as chamber pressure, RF power, substrate temperature, gas composition, and deposition time strongly influence the morphology and structural characteristics of the resulting VGNS [22–27]. Experimental studies have consistently shown that increasing plasma power enhances plasma density and ion bombardment, promoting vertical growth and improving electrolyte accessibility, whereas variations in chamber pressure and substrate temperature significantly affect nanosheet height, crystallinity, defect formation, and electrochemically accessible surface area [22–27]. These observations clearly demonstrate that the electrochemical behaviour of VGNS is intrinsically linked to the plasma conditions under which the material is synthesized, highlighting the importance of understanding the relationship between plasma characteristics, graphene growth, and electrode performance.

In addition to influencing the morphology of VGNS, the plasma environment also modifies the surface characteristics of the growing nanosheets, which directly affect their electrochemical behaviour. During PECVD, continuous ion bombardment and interactions with reactive plasma species generate structural defects, exposed graphene edges, and other surface features that alter the charge-storage characteristics of the electrode [28-31]. While excessive defect formation can disrupt the graphitic framework, an appropriate defect density creates electrochemically active sites that participate in reversible Faradaic reactions, thereby contributing to pseudocapacitive charge storage in addition to conventional electric double-layer capacitance (EDLC) [17,18,31–33]. Experimental studies have shown that the superior performance of plasma-grown VGNS results from the combined effects of their vertically interconnected architecture, which provides a large electrochemically accessible surface and facilitates efficient ion transport, together with plasma-induced edge defects that introduce additional electrochemically active sites [16–19,34,35]. These findings suggest that the electrochemical behaviour of VGNS is governed not only by the accessible surface area but also by the nature and density of plasma-induced active sites, highlighting the need to consider both morphology and surface activation when analysing charge-storage performance.

Although considerable progress has been made in the experimental growth and electrochemical characterization of VGNS, a clear quantitative understanding of how plasma operating conditions influence the final electrochemical performance is still evolving. Most experimental studies have examined the effects of individual processing parameters, such as chamber pressure, RF power, substrate temperature, and deposition time, on graphene growth and capacitance [22–27]. These investigations have provided valuable insight into the influence of plasma conditions on nanosheet morphology and electrode behaviour; however, they do not fully explain how changes in the plasma environment are translated into the electrochemical response of the electrode. Similarly, existing modelling studies have primarily focused on plasma transport or growth kinetics independently, with comparatively few attempts to integrate plasma characteristics, graphene growth, and electrochemical charge storage within a single framework [36-39]. Developing such a coupled modelling approach would not only improve the understanding of the mechanisms governing VGNS-based supercapacitors but also provide a practical means of selecting suitable PECVD operating conditions before undertaking extensive experimental studies.

In this work, a coupled plasma-assisted growth and electrochemical modelling framework is presented to quantitatively relate PECVD operating conditions to the electrochemical performance of vertically oriented graphene nanosheets (VGNS). Plasma characteristics obtained from a two-dimensional axisymmetric COMSOL model are combined with a reduced-order plasma-assisted growth model to describe the evolution of nanosheet height, thickness, and electrochemically accessible surface area under different processing conditions. These morphological characteristics are subsequently used in an electrochemical model that evaluates the contributions of electric double-layer capacitance (EDLC) and plasma-induced pseudocapacitance arising from electrochemically active sites. By integrating plasma transport, graphene growth, and electrochemical charge storage within a single framework, the present study provides a quantitative understanding of how plasma operating conditions influence the capacitance of VGNS electrodes and offers a useful computational tool for optimizing PECVD growth conditions for supercapacitor applications.

2. Mathematical Model

2.1 Plasma Transport Model

The plasma characteristics governing the growth of VGNS are obtained using a two-dimensional axisymmetric inductively coupled plasma (ICP) model developed in COMSOL Multiphysics. The plasma reactor consists of an $Ar/H/C_2H_2$ gas mixture operating under low-pressure PECVD conditions. The computational model solves the coupled equations governing electron continuity, electron energy transport, heavy-species transport, electrostatic potential, and plasma reaction kinetics to determine the spatial distributions of plasma species within the reactor [36].

The numerical solution provides the spatial distributions of electrons, ions, and reactive neutral species generated inside the plasma reactor under different PECVD operating conditions. These species determine the plasma chemistry responsible for graphene growth through adsorption, dissociation, ion bombardment, and surface reactions occurring at the catalyst surface. Since the complete plasma solution is available from the simulation, the concentrations of the individual reactive species are used directly in the growth calculations. However, the electron density (n_e) and electron temperature (T_e), are presented throughout this work as representative plasma parameters because they effectively describe the overall plasma state and facilitate comparison between different processing conditions [37].

2.2 Plasma-Assisted VGNS Growth Model

The growth of VGNS is governed by the interaction of reactive plasma species with the catalyst surface during PECVD [38]. Carbon-containing radicals generated in the discharge adsorb onto the catalyst and undergo a series of dissociation and surface diffusion processes, producing mobile carbon species that subsequently nucleate into graphene islands [28]. Continued incorporation of carbon atoms results in lateral expansion of these nuclei, while simultaneous hydrogen-assisted etching removes weakly bonded carbon and promotes structural ordering. As growth proceeds, the combined influence of surface stress and ion bombardment induces the transition from planar graphene domains to VGNS [29,30].

The evolution of the graphene morphology is described using a coupled plasma–surface interaction model that predicts the VGNS height, thickness, and areal density from the calculated plasma species fluxes. The present growth model is adapted from the framework reported in Ref. [36]. Rather than reproducing the full formulation, a reduced-order representation is used that retains the principal plasma–surface mechanisms controlling VGNS nucleation and morphology while providing the time-dependent variables required for the electrochemical calculations. Accordingly, the VGNS height (H), thickness (t), and collection currents of charged and neutral species obtained from the growth model are employed as the primary geometric descriptors of the electrode.

Equation (1) describes the evolution of the effective growth area of the VGNS [36]. The growth rate is governed by the balance between carbon incorporation at the sheet edges and the plasma-induced processes occurring at the graphene island surface.

$$L\partial_\tau\left(H\times t\right)=\left[\frac{4\,\overline{n}_C\,\pi D_{GI}}{\nu}D_0\exp\left(-\frac{\left(\Delta\varepsilon_{sd_C}\;+\Delta\varepsilon_{inc_C}\;\right)}{k_BT_s}\right)\frac{J_{iAGN}}{\pi D_{GI}^2}+\gamma_X J_{XGN}\right]\times \frac{M_{GN}}{\rho_{GN}}(1-\alpha_S\alpha_C), \tag{1}$$

where L denotes the average lateral dimension of the VGNS along the substrate surface, whereas t and H represent the VGNS thickness and vertical height, respectively. The height is measured normal to the substrate surface. In the present work, the values of H and t are obtained directly from the plasma-assisted growth model, where their evolution is governed by the coupled growth equations describing carbon incorporation and hydrogen-assisted etching [36], where J_{ijGN} and J_{jGN} (see Eqs. (2) and (3)) denote the collection currents of positively charged ions and carbon-containing neutral species reaching the growing VGNS surface, respectively. These quantities represent the ion-assisted and carbon incorporation fluxes that govern the plasma-assisted growth of the nanosheets. The continued growth of the VGNS is eventually limited by hydrogen-assisted etching of terminal carbon atoms at the sheet edges, resulting in the saturation of nanosheet growth and a gradual reduction in thickness. This behaviour is described by Eq. (4), in which the first and second terms account for the collection currents of positively charged hydrogen ions and neutral hydrogen species, respectively, incident on the VGNS surface. The complete description of Eqs. (1)–(4), together with the physical significance of each term and the definition of the species index j appearing in Eqs. (2) and (3), has been presented previously and is therefore not repeated here [28].

$$J_{ijGN}=n_{ij}\left(Lt+Ht+LH\right)\left(\frac{k_BT_{ij}}{2\pi^2m_{ij}}\right)^{\frac{1}{2}}\left\{\frac{2}{\sqrt{\pi}}\left(\frac{eV_s}{k_BT_i}\right)^{\frac{1}{2}}+\exp\left[\frac{eV_s}{k_BT_{ij}}\right]erfc\left[\left(\frac{eV_s}{k_BT_{ij}}\right)^{\frac{1}{2}}\right]\right\} \times\ \exp\left[-\frac{eU_s}{k_BT_s}\right], \tag{2}$$

$$J_{jGN}=n_j\left(Lt+Ht+LH\right)\left(\frac{k_BT_n}{2\pi^2m_j}\right)^{\frac{1}{2}} \tag{3}$$

$$\left[H\left(\tau\right)+L\right]\partial_\tau(t)=\left[\gamma_{iY}I_{iYGN}+\gamma_Y I_{YGN}\right]\overline{n}_H\,\frac{M_{GN}}{\rho_{GN}}\mathrm{H}(\tau), \tag{4}$$

The solution of above growth equations provides the temporal evolution of VGNS height (H), thickness (t), nuclei density, carbon collection current J_{XGN}, hydrogen collection current (J_{YGN}) and ion collection current (J_{ijGN}) corresponding to different plasma operating condition. These quantities form the link between plasma processing and electrochemical performance.

2.3 Electrochemical Performance Model

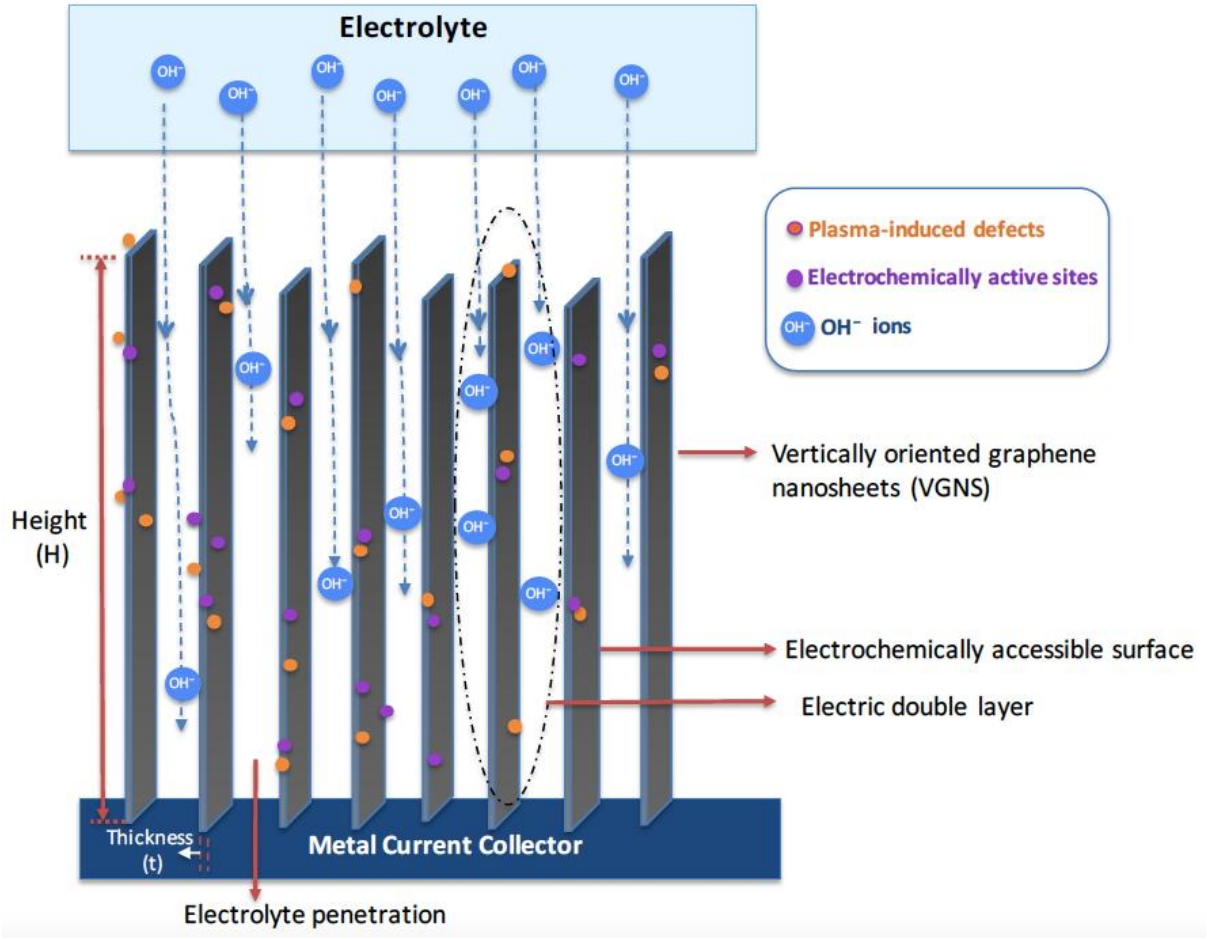


Figure1. Schematic illustration of a plasma-grown vertically oriented graphene nanosheet (VGNS) electrode immersed in an electrolyte.

Figure 1 schematically illustrates the plasma-grown vertically oriented graphene nanosheet (VGNS) electrode and the charge-storage mechanism considered in the present study. Hydroxide ions penetrate through the interconnected VGNS network, providing access to the electrochemically accessible surface area of the graphene nanosheets. Charge storage occurs through two complementary mechanisms: electric double-layer capacitance (EDLC), arising from the electrostatic adsorption of electrolyte ions on the graphene surface, and pseudocapacitance, originating from reversible Faradaic reactions at plasma-induced electrochemically active sites associated with structural defects. The combined contributions determine the overall capacitance of the VGNS electrode and form the basis of the electrochemical model developed in this work.

The electrochemical calculations are performed assuming a 6 M KOH aqueous electrolyte**,** which is widely employed for the characterization of VGNS-based supercapacitor electrodes owing to its high ionic conductivity and extensive experimental use in the literature [32-35].

As deposition proceeds, the continuous increase in VGNS height and density exposes additional graphene sidewalls to the electrolyte, thereby increasing the electrochemically accessible surface area. At any deposition time, the effective surface area (A_{eff}) is given by

$$A_{eff}(\tau) = A_o + 2N_s(\tau)H(\tau).\mathrm{L}\,A_o, \tag{5}$$

where A_0 is the projected substrate area, $H(\tau)$ is the corresponding VGNS height predicted by the growth model and L is the average lateral sheet length. The growth model provides the normalized nuclei population, which is converted into the physical VGNS areal density, $N_s(\tau)$, using the reference density defined in Ref. [36]. The physical value of $N_s(\tau)$ is subsequently used in the effective-area and electrode-mass calculations. Here, the second term represents the additional surface area contributed by the two exposed faces of the VGNS.

The mass of the deposited graphene is determined from the predicted VGNS geometry as

$$m(\tau) = \rho_C N_s(\tau)H(\tau)Lt(\tau)A_0, \tag{6}$$

where ρ_C ($\approx$2.26 g cm^{-3}) is the density of graphitic carbon [40,41] and *t(τ)* is the VGNS thickness predicted by the growth model. In this way, the electrode mass increases continuously with deposition time rather than being assumed constant.

During PECVD growth process of VGNS, energetic ion bombardment introduces structural defects into the VGNS structure, while the continuous arrival of carbon species promotes graphitic growth [29]. To represent the balance between these competing processes, the normalized defect density is expressed as

$$N_d(\tau) = 1 - \exp\left[-k_d\left(\frac{J_{ijGN}(\tau)}{J_{XGN}(\tau)}\right)\right], \tag{7}$$

where J_{ijGN} and J_{XGN} denote the ion and carbon collection currents (see Eqs. (2) and (3)) predicted by the growth model, respectively, and k_d ($\approx$ 1.0) is the defect-generation coefficient. Equation 7 reflects the increase in defect density with increasing ion bombardment relative to carbon incorporation.

Not all structural defects generated during plasma-assisted growth contribute equally to electrochemical charge storage [31]. Only a fraction of these defects act as electrochemically active sites that participate in reversible faradaic reactions. Accordingly, the normalized active-site density is expressed as

$$N_a(\tau) = 1 - \exp\left[-k_a N_d(\tau)\right], \tag{8}$$

where N_d and N_a are the normalized defect density and active-site density, respectively, and k_a(=1.5) is the activation coefficient governing the conversion of structural defects into electrochemically active sites. Both N_d and N_a vary between zero and unity. The exponential form of Eq. (8) accounts for the gradual saturation of active sites as the number of available

defect locations decreases with continued deposition. The electrical double-layer capacitance ($C_{DL}(\tau)$) being a non-faradaic, electrostatic mechanism, depends on accessible surface area alone and therefore,

$$C_{DL}(\tau) = C_A A_{eff}(\tau), \tag{9}$$

where A_{eff} is the effective electrochemically accessible surface area predicted by the growth model and C_A is the intrinsic areal capacitance of the graphene–electrolyte interface. In the present work, C_A=0.20 Fm^{-2} is adopted, which lies within the experimentally reported range for graphitic carbon electrodes in aqueous alkaline electrolytes [32–35]. Since C_A is an intrinsic interfacial property, it is assumed to remain constant, and variations in the electric double-layer capacitance arise solely from plasma-induced changes in the accessible surface area.

The pseudocapacitive contribution originates from reversible faradaic reactions occurring at plasma-generated electrochemically active sites. It is expressed as

$$C_P(\tau) = C_{P,A} C_{DL}(\tau) N_a(\tau), \tag{10}$$

where $C_{P,A}$ (Fm^{-2}) is the intrinsic pseudocapacitance per unit effective surface area associated with fully activated graphene. Thus, the pseudocapacitance increases with both the accessible surface area and the density of electrochemically active sites generated during plasma-assisted growth.

The total capacitance of the VGNS electrode is obtained by combining the electric double-layer and pseudocapacitive contributions,

$$C_T(\tau) = C_{DL}(\tau) + C_P(\tau), \tag{11}$$

The corresponding specific capacitance is calculated as

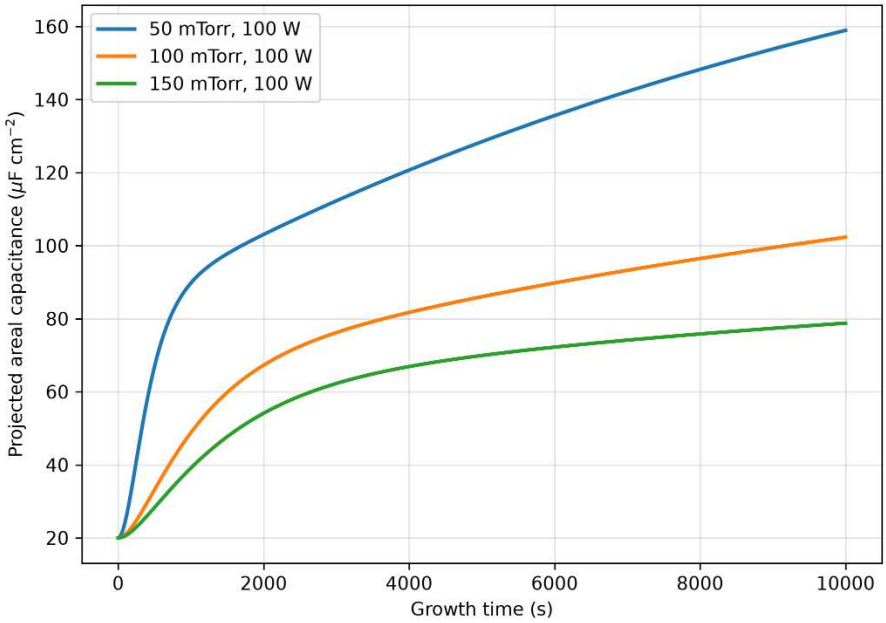
$$C_s(\tau) = \frac{C_T(\tau)}{m(\tau)}, \tag{12}$$

In addition to the gravimetric specific capacitance, the projected areal capacitance $C_{proj}(\tau) = \frac{C_T(\tau)}{A_0}$ is adopted as the primary metric for evaluating the electrochemical performance of VGNS electrodes throughout this work, as it provides the most appropriate basis for comparison with experimentally reported plasma-grown graphene electrodes.

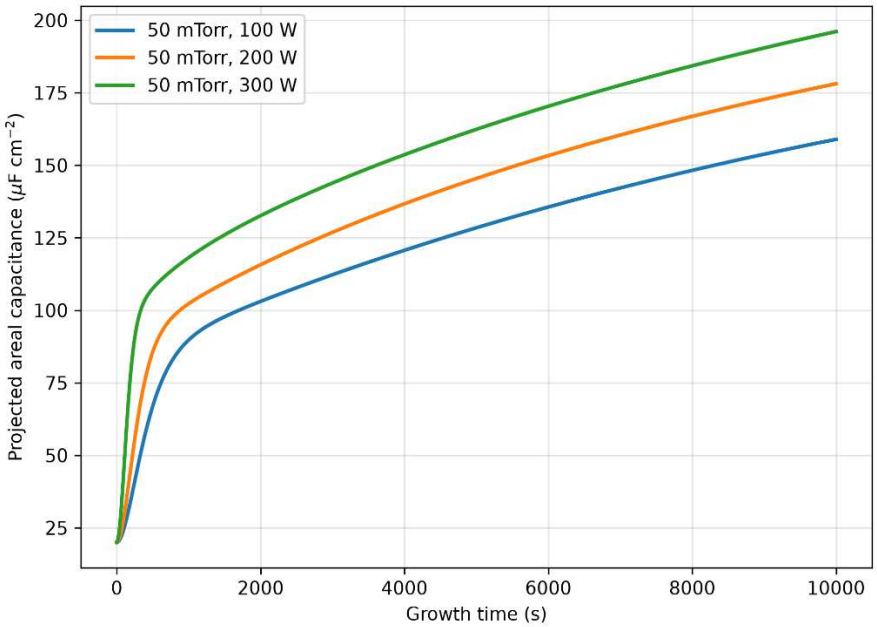
3. Results and Discussion

The electrochemical performance of VGNS synthesized under different PECVD operating conditions was investigated using the coupled plasma-growth-capacitance framework developed in this work. Plasma characteristics inside the reactor were obtained using the Inductively Coupled Plasma (ICP) module of COMSOL Multiphysics 5.2a, whereas the VGNS growth model, electrochemical calculations, parameter optimization, sensitivity analysis, and graphical visualization were implemented in Python 3.12. This integrated

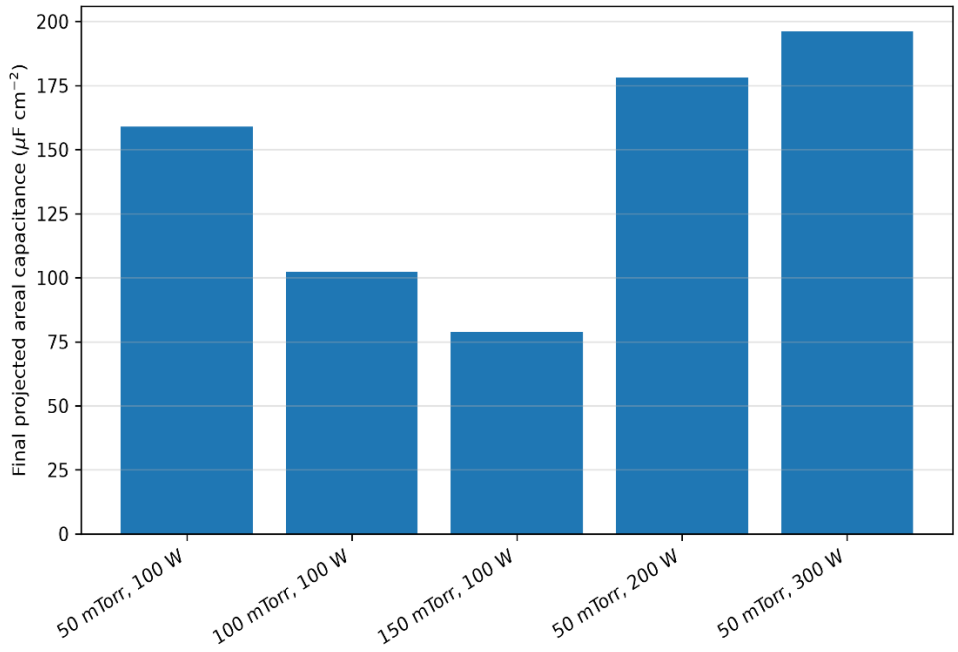
methodology establishes a direct relationship between the plasma environment inside the reactor and the resulting electrochemical performance of the graphene electrode.



(a)



(b)



(c)

Figure 2. Evolution of projected areal capacitance with growth time (a) at different chamber pressures (RF power=100 W) and (b)at different RF powers (chamber pressure=50 mTorr). (c) Final projected areal capacitance under different operating conditions.

Pressure (mTorr)	RF Power (W)	(n_e) ($\times 10^{17}$ m^{-3})	(T_e) (eV)	Height (nm)	Thickness (nm)
150	100	0.028	1.05	104	5.27
100	100	0.135	1.78	188	5.11
50	100	0.66	2.51	334	4.99
50	200	1.50	2.74	382	4.94
50	300	5.15	3.20	443	4.86

Table 1. Predicted plasma characteristics and VGNS morphological parameters obtained from the plasma-assisted growth model under different PECVD operating conditions. These quantities are subsequently used as inputs for the electrochemical performance model.

The evolution of the projected areal capacitance during graphene growth is presented in Fig. 2. Irrespective of the plasma operating condition, the capacitance increases continuously with deposition time before gradually approaching a nearly steady value. The rapid increase observed during the initial stage of deposition is associated with the continuous formation of graphene nuclei and the rapid expansion of electrochemically accessible surface area [42]. As growth proceeds, the graphene architecture gradually approaches a stable morphology, resulting in a slower increase in capacitance, consistent with the saturating relationship between PECVD deposition time and electroactive surface area reported for structurally related vertically aligned carbon films [43]. Such behaviour indicates that most of the

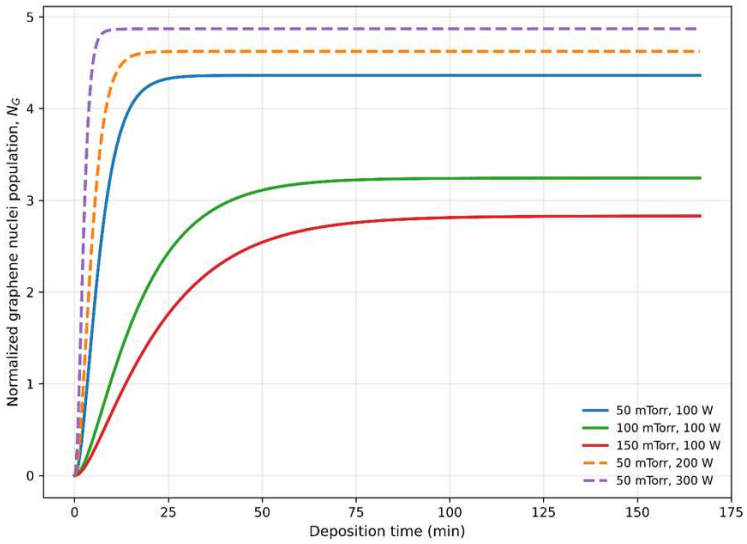
electrochemically active surface has already been developed during the later stages of deposition, and therefore only marginal improvements in charge-storage capability are obtained with further growth, consistent with the existence of an optimal plasma exposure duration beyond which further treatment does not continue to improve performance, as reported for plasma-treated graphene-based electrodes more generally [44].

The influence of chamber pressure on capacitance evolution is shown in Fig. 2(a). At a constant RF power of 100 W, the VGNS electrode synthesized at 50 mTorr exhibits the highest capacitance throughout the deposition process, whereas increasing the chamber pressure progressively suppresses the electrochemical response. By the end of the deposition period, the projected areal capacitance decreases from approximately 159 μF cm^{-2} at 50 mTorr to 102 μF cm^{-2} and 79 μF cm^{-2} at 100 mTorr and 150 mTorr, respectively. The progressive separation of the three curves indicates that the influence of plasma pressure becomes increasingly significant as the VGNS structure develops. Reducing the chamber pressure increases both the electron density and electron temperature near the substrate (see Table 1), enabling more efficient methane dissociation and generating a larger flux of reactive carbon species and energetic ions. In the coupled growth model, these conditions favour the formation of taller VGNS (shown in Fig. 3(b)) while simultaneously promoting defect generation through enhanced ion bombardment [45,46]. The larger VGNS surface increases the electric double-layer capacitance, whereas the additional plasma-induced defects create more electrochemically active sites [see Fig. 4] that contribute to pseudocapacitive charge storage, consistent with the defect-density-dependent capacitance mechanism established for graphene electrodes generally [47] and directly demonstrated for vertically oriented versus planar graphene grown under otherwise identical plasma conditions [48].

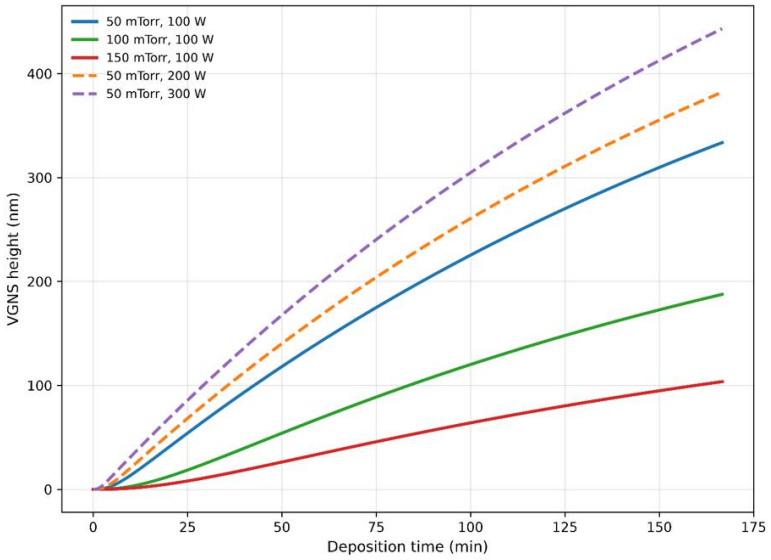
A similar trend is observed when the RF power is increased while maintaining the chamber pressure at 50 mTorr, as shown in Figure 2(b). Increasing RF power enhances the projected areal capacitance 159 cm^{-2}, 178 μF cm^{-2}, and 196 μF cm^{-2} at 100 W, 200 W, and 300 W, respectively. The continuous increase in capacitance reflects the progressively more energetic plasma generated at higher RF powers. As will be discussed in Table 1, increasing RF power increases both the electron density and electron temperature near the substrate, thereby enhancing methane dissociation, ion bombardment and the supply of reactive carbon species [37,49], which experimentally has been shown to control nanowall density and electrical properties in PECVD systems [50]. These conditions drive both taller VGNS growth and a higher density of plasma-induced defects (see Figs. 3 and 4.), increasing the electrochemically accessible surface area and the density of electrochemically active sites (see Fig. 4), consistent with the general mechanism by which plasma-modified graphene electrodes achieve enhanced capacitance [48, 51, 52].

The combined influence of chamber pressure and RF power on the final projected capacitance is summarized in Fig. 2(c). Among all the operating conditions investigated, the highest projected capacitance is obtained at 50 mTorr and 300 W, whereas the lowest value corresponds to 150 mTorr and 100 W. Overall, reducing the chamber pressure and increasing the RF power lead to a systematic increase in the projected capacitance. These observations clearly demonstrate that plasma operating conditions play a decisive role in determining the electrochemical performance of VGNS electrodes. The model predicts a maximum projected capacitance of approximately 196 μF cm^{-2}, which is in good agreement with the experimentally reported value of 197 μF cm^{-2} for plasma-grown VGNS electrodes under similar electrochemical conditions [48]. The close agreement indicates that the proposed model captures the dominant physical mechanisms governing the capacitance of VGNS electrodes.

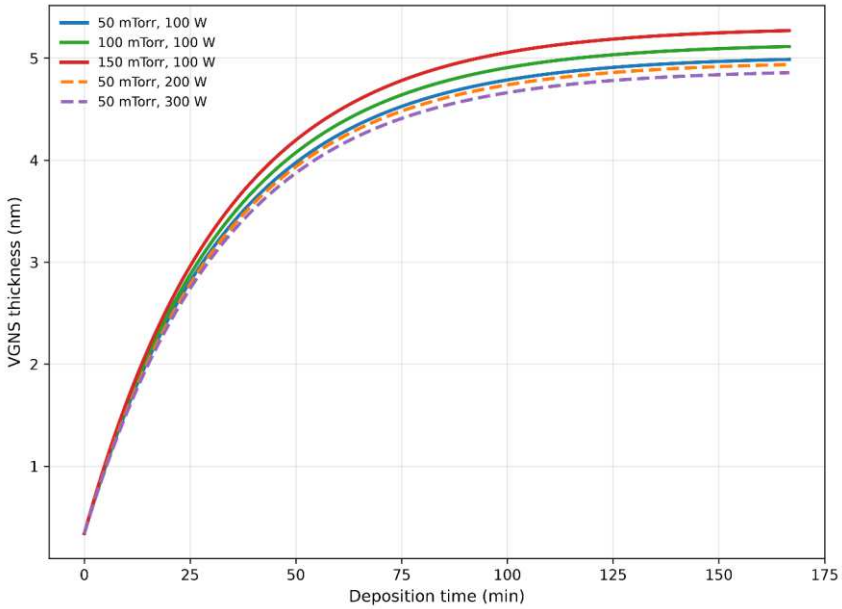
The improvement in electrochemical performance presented in Fig. 2 is closely related to the plasma conditions established during VGNS growth. In a PECVD process, the plasma not only supplies the reactive carbon species required for graphene formation but also governs the ion bombardment experienced by the growing surface [46]. Consequently, any change in the operating pressure or RF power alters the plasma characteristics [29] and ultimately influences the morphology of the deposited graphene [28]. The corresponding plasma parameters predicted by the COMSOL model, together with the resulting final VGNS morphology are summarized in Table 1, while the corresponding growth kinetics are illustrated in Fig. 3. The Table 1 provides the near-substrate plasma characteristics together with the final morphological parameters predicted by the coupled model, whereas the time-dependent curves reveal how the graphene structure develops throughout the deposition process. Presenting both the final values and their temporal evolution provides a comprehensive understanding of the growth mechanism and enables the relationship between plasma conditions and graphene morphology to be clearly established.



(a)



(b)



(c)

Figure 3. Time evolution of (a) normalized graphene nuclei population, (b) graphene sheet height, and (c) graphene sheet thickness under different PECVD operating conditions. The pressure sweep was performed at a constant RF power of 100 W, whereas the RF-power sweep was carried out at a constant chamber pressure of 50 mTorr.

The early stages of graphene growth are governed by the formation and development of graphene nuclei, as illustrated in Fig. 3(a). Under all plasma operating conditions, the normalized nuclei population increases rapidly during the initial deposition period before gradually approaching a stable value, indicating the establishment of a steady growth regime. However, the nucleation behaviour is strongly influenced by the plasma conditions. At a constant RF power of 100 W, increasing the chamber pressure progressively slows nuclei development and reduces the final nuclei population. This behaviour agrees well with the experimental observations of Cho et al. [54], who reported that higher operating pressures suppress graphene nucleation by reducing the concentration of reactive growth species. In contrast, increasing the RF power from 100 to 300 W at a fixed chamber pressure of 50 mTorr accelerates nuclei formation and results in a larger equilibrium nuclei population. Similar enhancements in graphene nucleation with increasing plasma power have been reported by Ma et al. [55] and Jafari et al. [56], who attributed this behaviour to more efficient precursor dissociation and an increased flux of reactive carbon radicals. The predicted trend is also supported by the plasma characteristics summarized in Table 1, where lower chamber pressures and higher RF powers produce higher electron densities and electron temperatures, in agreement with the plasma behaviour reported by Lieberman and Lichtenberg [37], Mao et al. [53], and Collison et al. [57]. The increase in electron density and electron temperature enhances the electron-impact dissociation of hydrocarbon gas, generating a larger concentration of carbon-containing reactive species that participate in graphene nucleation and subsequently promote the growth of VGNS.

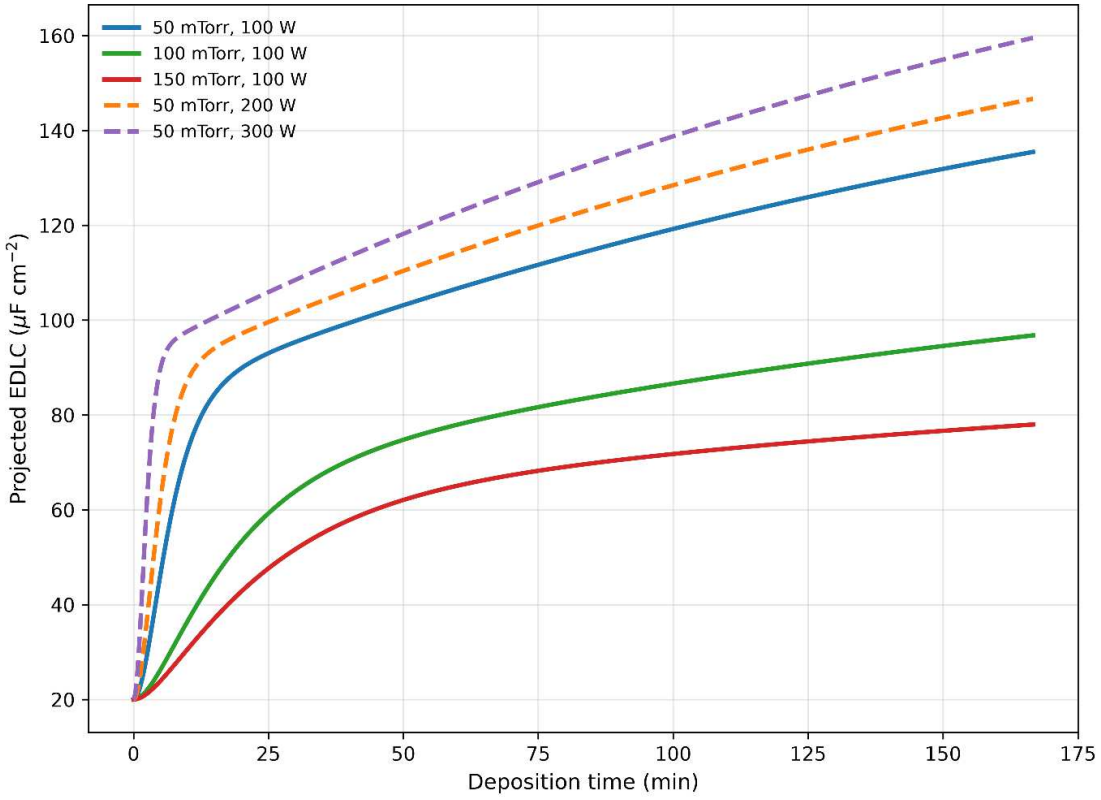
The evolution of graphene height closely follows the nucleation behaviour, as illustrated in Fig. 3(b). In every case, the VGNS height increases rapidly during the initial stages of deposition and subsequently continues to grow at a slower rate as the growth process

approaches saturation. Although the overall growth profile remains similar, the final height depends strongly on the plasma operating conditions. Increasing the chamber pressure progressively suppresses VGNS height, whereas increasing the RF power promotes continuous vertical growth throughout the deposition period. The corresponding final values summarized in Table 1 follow the same trend and are in good agreement with the experimental observations reported by Cho et al. [54] and Takeuchi et al.[58], who demonstrated that higher operating pressures hinder the formation of well-developed vertically oriented graphene structures. Conversely, the enhancement in graphene height with increasing RF power is consistent with the findings of Ma et al. [55] and Jafari et al. [56], where higher plasma power was shown to promote more efficient precursor dissociation and faster vertical graphene growth.

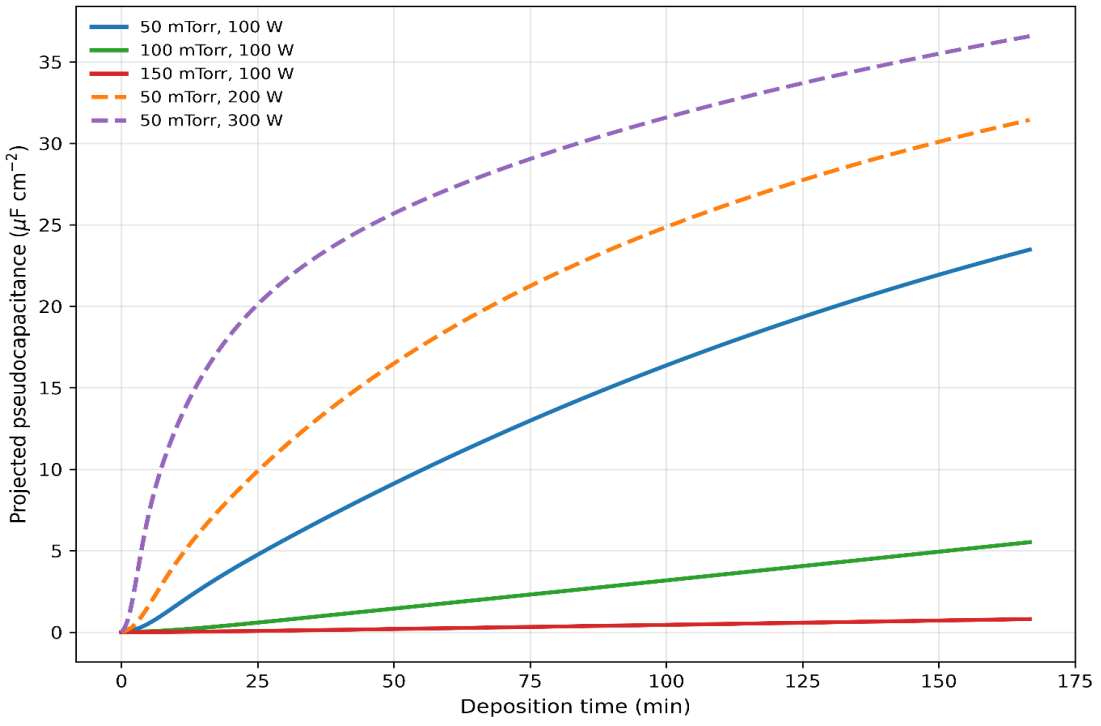
The observed behaviour can be attributed to the changes in the near-substrate plasma characteristics under different operating conditions. As summarized in Table 1, lower chamber pressures and higher RF powers produce higher electron densities and electron temperatures, leading to more efficient electron-impact dissociation of acetylene and a greater flux of reactive carbon species arriving at the growth surface. The increased availability of these reactive species accelerates carbon incorporation at the graphene edges, thereby favouring vertical sheet extension over the entire deposition period. In contrast, increasing the chamber pressure reduces plasma activity, limiting precursor dissociation and slowing the vertical growth process. This morphology is particularly advantageous for supercapacitor electrodes. Taller VGNS expose a larger electrochemically accessible surface while preserving open channels for electrolyte penetration and rapid ion transport. Such an architecture has been shown to improve electric double-layer charge storage, as first demonstrated by Miller et al. [59] and later confirmed experimentally for vertically oriented graphene electrodes by Ghosh et al. [48]. Consequently, the enhanced vertical growth predicted under low-pressure and high-power conditions provides a direct structural basis for the higher capacitance observed in Fig. 2.

A different response is observed for the VGNS thickness, as presented in Fig. 3(c). Unlike the continuous increase in height, the thickness rises rapidly during the initial deposition stage and then gradually approaches a nearly constant value. The influence of the plasma conditions on thickness is considerably less pronounced than that observed for VGNS height. The final thickness values summarized in Table 1 reveal two distinct trends. Increasing the chamber pressure leads to a gradual increase in sheet thickness, whereas increasing the RF power produces a slight reduction. These trends can be understood from the changes in the near-substrate plasma characteristics. At higher chamber pressures, the electron density and electron temperature decrease, resulting in a less energetic plasma. The reduced ion bombardment and weaker hydrogen-assisted edge etching allow a larger fraction of the deposited carbon to accumulate along the graphene edges, promoting lateral thickening of the VGNS. In contrast, increasing the RF power generates a denser and more energetic plasma, which enhances hydrogen-assisted etching and ion-induced surface reactions. Under these conditions, carbon incorporation is directed preferentially towards vertical extension of the graphene sheets rather than lateral growth, giving rise to relatively thinner VGNS. Therefore, from Figs. 3(b) and 3(c), we conclude that lower chamber pressures and higher RF powers produce VGNS with a larger height-to-thickness ratio, resulting in high-aspect-ratio VGNS. Such architectures provide a larger electrochemically accessible surface while maintaining open channels for electrolyte penetration and rapid ion transport. The beneficial effect of high-aspect-ratio vertically oriented graphene on charge-storage performance has been

demonstrated experimentally by Miller et al. [59] and further confirmed by Ghosh et al. [48], who showed that vertically oriented graphene electrodes exhibit significantly improved double-layer capacitance compared with planar graphene.



(a)



(b)

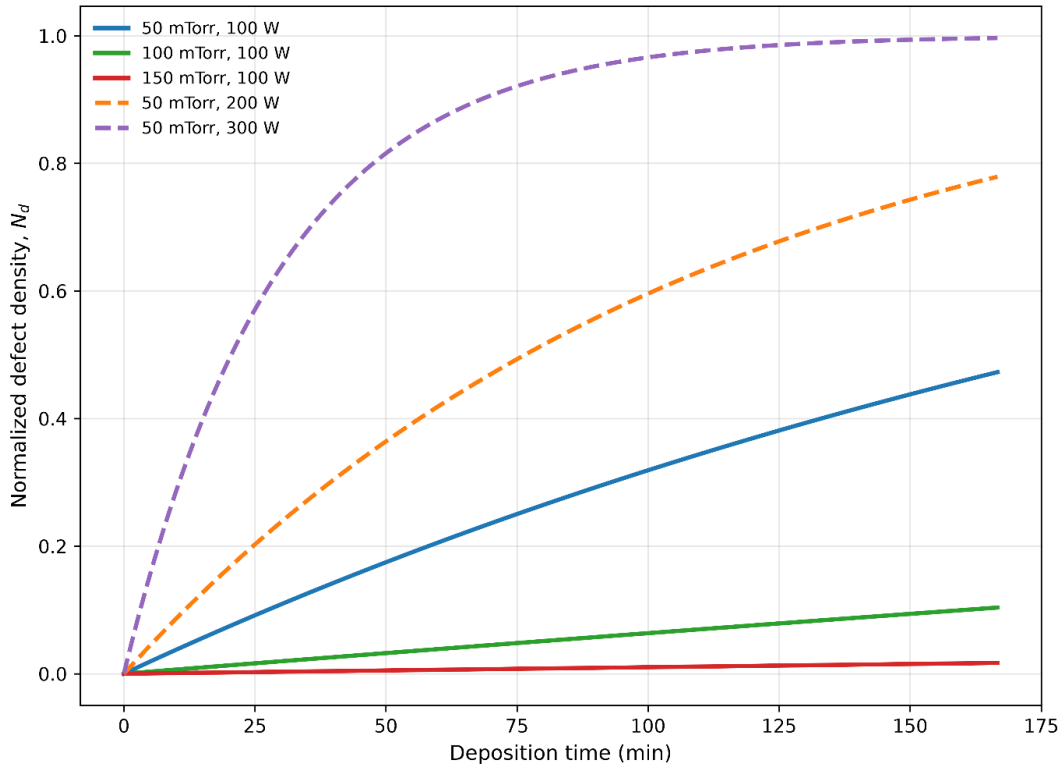
Figure 4. Time evolution of (a) projected electric double-layer capacitance (EDLC), (b) projected pseudocapacitance. Solid lines correspond to the pressure sweep at a constant RF power of 100 W, whereas dashed lines represent the RF-power sweep performed at a constant chamber pressure of 50 mTorr.

The results presented so far demonstrate that under favourable plasma conditions, the growth of high-aspect-ratio VGNS creates a vertically aligned, interconnected network that exposes a larger electrochemically accessible surface area while providing open pathways for efficient electrolyte penetration and rapid ion transport. Simultaneously, plasma-induced surface activation generates structural defects that subsequently evolve into electrochemically active sites, contributing additional faradaic charge storage. The superior electrochemical performance predicted under low-pressure and high-power conditions therefore arises from the combined effects of a high-aspect-ratio graphene architecture and plasma-induced surface activation, rather than from either mechanism acting independently. To distinguish the individual contributions of these two charge-storage mechanisms, the total projected areal capacitance predicted by the coupled model was separated into its electric double-layer and pseudocapacitive components, as shown in Fig. 4. The electric double-layer capacitance is governed primarily by the accessible surface area provided by the high-aspect-ratio VGNS, whereas the pseudocapacitive contribution depends on the density of plasma-induced electrochemically active sites.

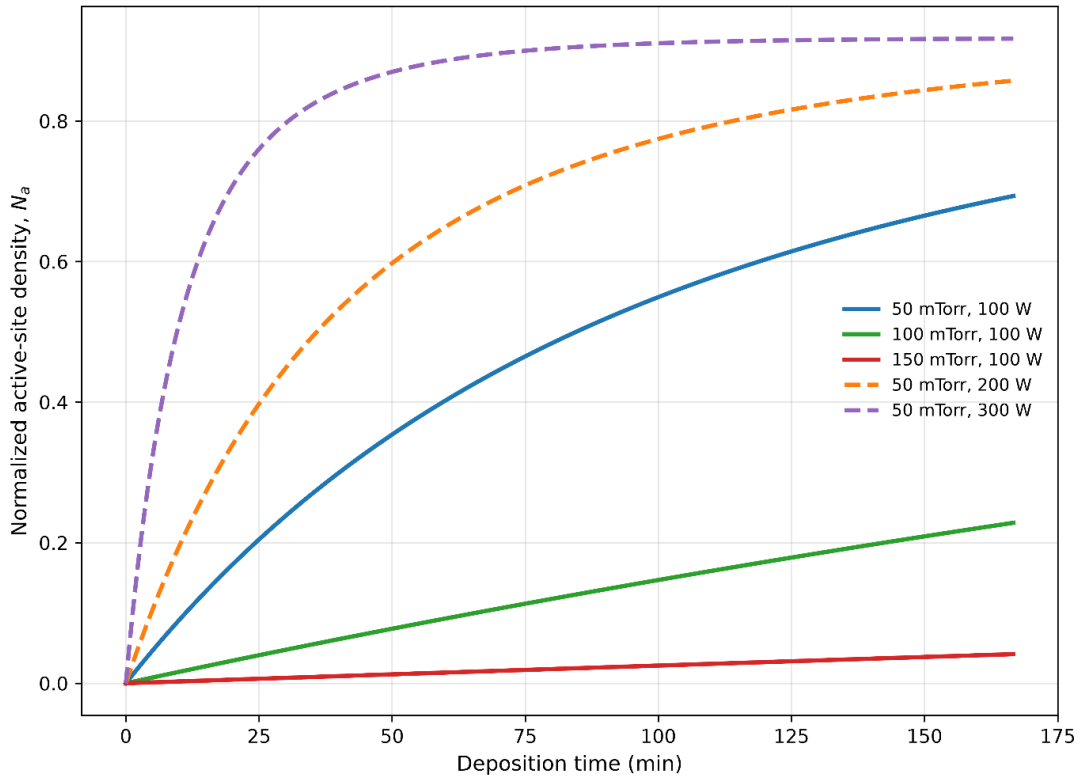
The evolution of the projected EDLC is presented in Fig. 4(a). Under all operating conditions, the EDLC increases steadily throughout the deposition process before gradually approaching a stable value as graphene growth reaches completion. Lower chamber pressures and higher RF powers consistently produce larger EDLC values, indicating that favourable plasma conditions enhance electric double-layer charge storage. This behaviour closely follows the evolution of graphene height shown in Fig. 3(b), confirming that the EDLC is primarily controlled by the development of the vertically oriented graphene architecture. The development of taller, high-aspect-ratio VGNS provide a larger electrochemically accessible surface while preserving open channels for electrolyte penetration and rapid ion transport, thereby facilitating greater charge accumulation at the electrode–electrolyte interface. Similar behaviour has been reported experimentally for VGNS electrodes, where the combination of a high-aspect-ratio architecture and improved electrolyte accessibility leads to superior electric double-layer charge storage compared with conventional planar graphene electrodes [48,59].

The evolution of the projected pseudocapacitance is presented in Fig. 4(b). Under all operating conditions, the pseudocapacitive contribution increases rapidly during the initial stage of deposition before gradually approaching saturation, with the highest values consistently obtained at lower chamber pressures and higher RF powers. Unlike the EDLC, which is governed primarily by the electrochemically accessible surface area, the pseudocapacitive response is controlled by plasma-induced surface activation. The origin of this behaviour can be understood from the evolution of the normalized defect density and active-site density shown in Figs. 5(a) and 5(b), respectively. As illustrated in Fig. 5(a), favourable plasma conditions generate a higher density of structural defects because the increased electron density and electron temperature (Table 1) promote more energetic ion bombardment and enhanced hydrocarbon dissociation during graphene growth[45,46]. These

plasma-induced defects subsequently evolve into electrochemically active sites, causing the active-site density in Fig. 5(b) to closely follow the defect-density trend. The increase in active sites provides additional locations for reversible ion adsorption and surface charge-transfer reactions, leading to a corresponding enhancement in the pseudocapacitive contribution. Consequently, the operating conditions that produce the highest defect and active-site densities also exhibit the largest pseudocapacitance. The close agreement between the trends observed in Figs. 4 and 5 demonstrates that plasma-induced defect generation enhances the pseudocapacitive behaviour indirectly by increasing the density of electrochemically active sites. The predicted relationship is consistent with experimental observations reported for plasma-grown VGNS. he predicted relationship is consistent with experimental observations reported for plasma-grown vertically oriented graphene. Previous studies have shown that energetic ion bombardment during plasma processing generates a high density of edge defects, which subsequently act as electrochemically active sites for charge storage [45,46]. Yang *et al.* [17] further demonstrated that the edge-rich architecture of vertically oriented graphene provides abundant electrochemically active sites, leading to enhanced pseudocapacitive behaviour and improved overall charge-storage performance. Similarly, Ghosh *et al.* [48] reported that vertically oriented graphene synthesized under plasma conditions possessed a substantially higher defect density than planar graphene and exhibited significantly greater areal capacitance. These experimental findings collectively support the mechanism proposed in the present model, where plasma-induced defect generation increases the density of electrochemically active sites, thereby enhancing the pseudocapacitive contribution through faradaic charge-storage processes

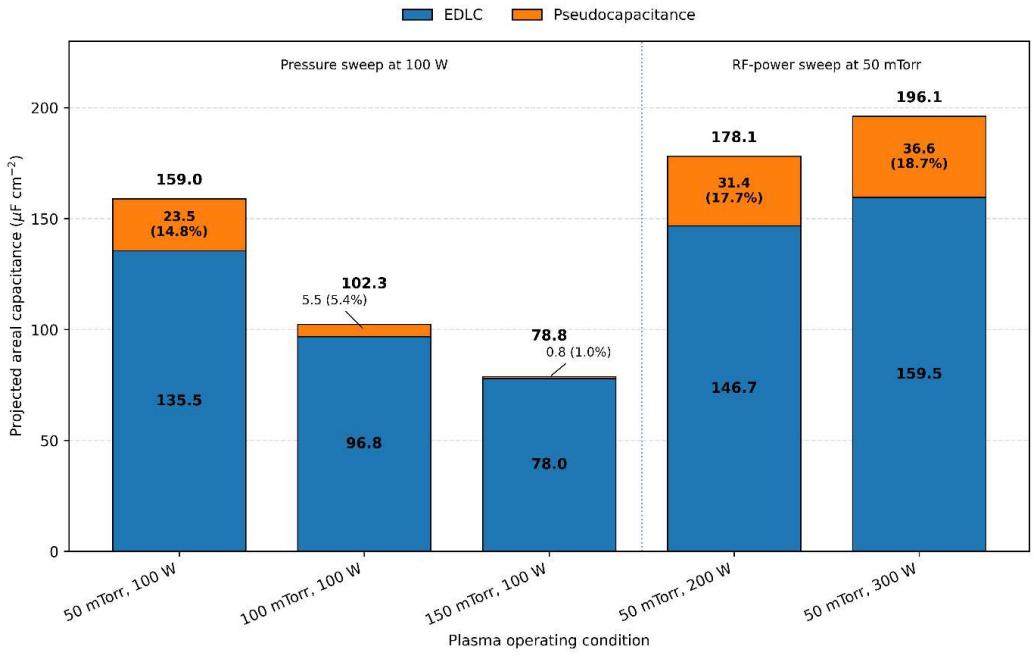


(a)

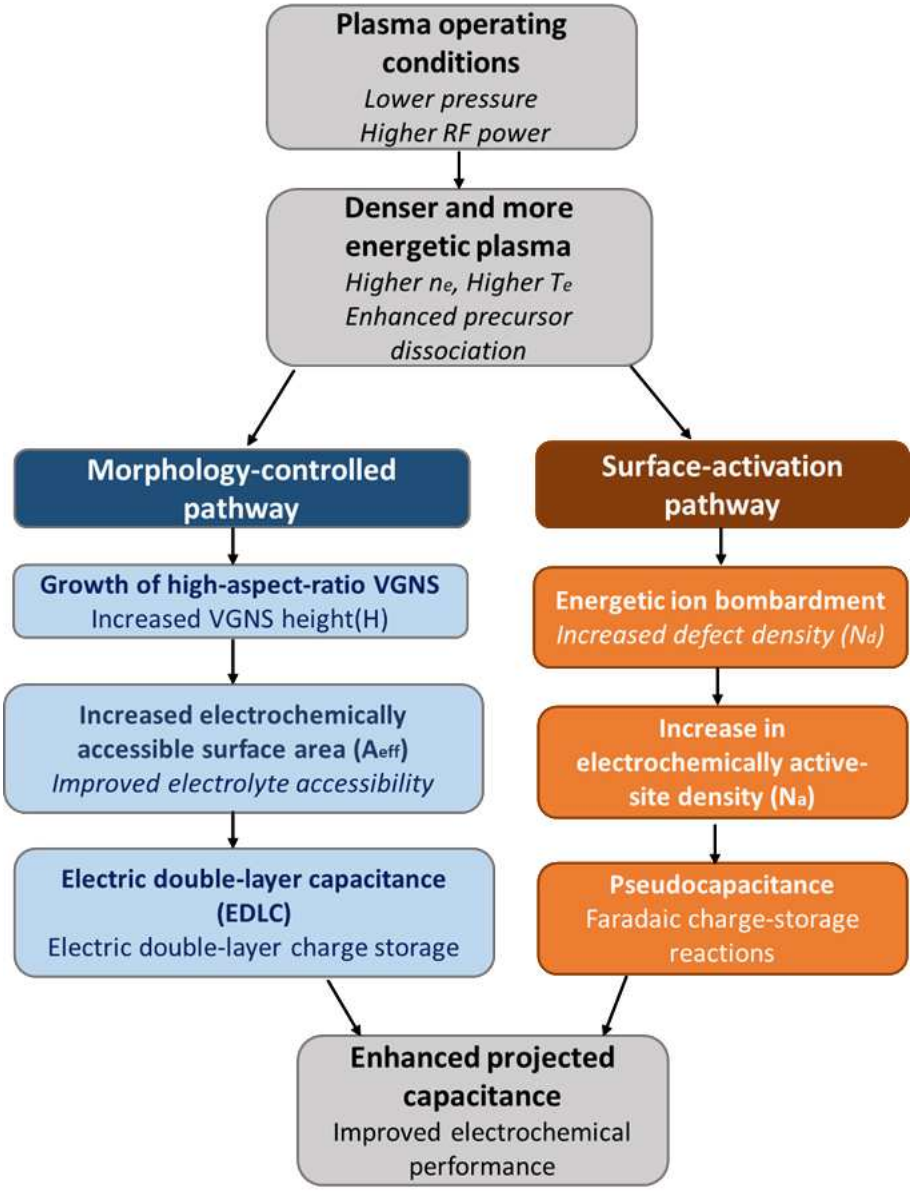


(b)

Figure 5. Time evolution of (a) normalized defect density (N_d) and (b) normalized electrochemically active-site density (N_a) predicted under different PECVD operating conditions. The pressure sweep was performed at a constant RF power of 100 W, whereas the RF-power sweep was carried out at a constant chamber pressure of 50 mTorr.



(a)



(b)

Figure 6 (a) Relative contributions of EDLC and pseudocapacitance to the final projected capacitance under different plasma operating conditions. (b) Proposed coupled plasma–growth–electrochemical mechanism illustrating the simultaneous effects of plasma-assisted graphene growth and surface activation on the charge-storage behaviour of VGNS.

The individual effects of graphene morphology and plasma-induced surface activation have been discussed through the preceding results. However, the enhanced electrochemical performance of the VGNS electrode cannot be attributed to either of these factors alone. Instead, it results from their combined influence during plasma-assisted growth. To provide an overall understanding of this coupled plasma–growth–electrochemical model, Fig. 6 summarizes the final contributions of the electric double-layer capacitance (EDLC) and

pseudocapacitance under different plasma operating conditions and illustrates the overall mechanism responsible for the enhanced charge-storage behaviour.

As shown in Fig. 6(a), both the EDLC and pseudocapacitive contributions increase with decreasing chamber pressure and increasing RF power, resulting in a corresponding enhancement in the total projected capacitance. The EDLC remains the dominant charge-storage mechanism throughout the investigated operating range, accounting for approximately 99% of the total capacitance at 150 mTorr and 100 W, while contributing about 81% at 50 mTorr and 300 W. In contrast, the relative contribution of pseudocapacitance increases from approximately 1% to nearly 19% over the same operating conditions. Although the electric double-layer mechanism continues to provide the major share of charge storage, the increasing pseudocapacitive contribution clearly indicates that plasma-induced surface activation becomes progressively more significant under favourable plasma conditions. This behaviour confirms that the enhanced electrochemical performance of the VGNS electrode arises from the simultaneous improvement of both electric double-layer and pseudocapacitive charge-storage mechanisms.

The overall mechanism responsible for this behaviour is illustrated schematically in Fig. 6(b). Under lower chamber pressures and higher RF powers, the plasma becomes denser and more energetic, leading to higher electron density, higher electron temperature and more efficient precursor dissociation. These plasma conditions simultaneously promote the growth of high-aspect-ratio VGNS and the generation of structural defects through energetic ion bombardment. The taller graphene architecture increases the electrochemically accessible surface area available for electric double-layer charge storage, while the plasma-induced defects evolve into electrochemically active sites that enhance the pseudocapacitive response. Experimental studies on plasma-grown vertically oriented graphene have reported similar behaviour, where the edge-rich architecture and defect-rich surface contribute simultaneously to enhanced electrochemical activity and improved capacitance [17,45,46,48].

Overall, the coupled plasma–growth–electrochemical model demonstrates that the electrochemical performance of plasma-grown VGNS is governed by the cooperative interaction between graphene morphology and surface chemistry. By linking plasma operating conditions with graphene growth, defect generation and charge-storage behaviour within a single framework, the present model provides a mechanistic understanding of plasma-assisted graphene synthesis and offers useful guidelines for optimizing growth conditions for high-performance supercapacitor electrodes.

4. Conclusion

In this work, a coupled plasma-assisted growth and electrochemical model has been developed to establish a direct relationship between PECVD operating conditions and the supercapacitor performance of VGNS. By integrating plasma transport, graphene growth kinetics and electrochemical charge-storage mechanisms, the model provides a physically consistent framework for predicting how plasma processing influences electrode morphology and capacitance. The results demonstrate that decreasing the chamber pressure and increasing the RF power promote the growth of taller VGNS with a larger electrochemically accessible surface area, while simultaneously increasing the density of plasma-induced defects and electrochemically active sites. Consequently, both the electric double-layer capacitance and pseudocapacitance increase under more energetic plasma conditions. Although electric double-layer capacitance remains the dominant charge-storage mechanism (approximately 81–99% of

the total capacitance), the increasing pseudocapacitive contribution highlights the important role of plasma-induced surface activation in enhancing the overall electrochemical performance. Among the conditions investigated, the highest projected capacitance of approximately 196 μF cm^{-2} was obtained at 50 mTorr and 300 W, in good agreement with reported experimental values for plasma-grown VGNS electrodes.

Overall, the proposed model demonstrates that the superior electrochemical performance of VGNS electrodes results from the combined effects of morphology-induced surface-area enhancement and plasma-induced surface activation. The developed framework provides a useful computational tool for understanding and optimizing plasma-assisted synthesis of graphene electrodes and offers a rational approach for selecting suitable PECVD operating conditions prior to experimental fabrication. Future work will focus on incorporating more detailed plasma chemistry and comprehensive experimental validation to further improve the predictive capability of the model.

Research Funding

No funds, grants, or other support was received.

References

[1] M. Salaheldeen, T. N. A. Eskander, M. Fathalla, , V. Zhukova, , J. M. Blanco, J. Gonzalez, , A. Zhukov, and A. M. Abu-Dief, *Batteries 11,* 232 (2025).

[2] J. Zhang, M. Gu, and X. Chen, Micro and Nano Engineering **21**, 100229 (2023).

[3] R. K. Azega et al. **41**, e01111(2024).

[4] H. Rashid Khan and A. Latif Ahmad, Journal of Industrial and Engineering Chemistry **141**, 46 (2025).

[5] S. Mishra, R. Srivastava, A. Muhammad, A. Amit, E. Chiavazzo, M. Fasano, and P. Asinari, Scientific Reports **13**, 6494 (2023).

[6] L. Liu, X. Qin, and R. Zhang, Smart Mater Devices, 1:202504 (2025), doi: 10.70401/smd.2025.0008.

[7]]M. Zhong, M. Zhang, and X. Li, Carbon Energy **4**, 950 (2022).

[8] P. K. Sahoo, N. Kumar, A. Jena, S. Mishra, C.-P.Lee, S.-Y. Lee, S.-J. Park, RSC Adv. **14** 1284 (2024).

[9] A. K. Geim & K. S. Novoselov, Nature Materials **6**, 183 (2007).

[10] M. D. Stoller, S.Park, Y. Zhu, J. An, R. S. Ruoff, **Nano Letters 8**, 3498 (2008).

[11] C. Lee, X. Wei, J. W. Kysar, and J. Hone, **Science 321**, 385 (2008).

[12] R. R. Nair, P. Blake, A. N. Grigorenko, K. S. Novoselov, T. J. Booth, T. Stauber, N. M. R. Peres, and A. K. Geim, Science **320**,1308 (2008).

[13] X. Yang, J. Zhu, L. Qiu, and D. Li, Advanced Materials **23**, 2833 (2011).

[14] C. Liu, Z. Yu, D. Neff, A. Zhamu, and B. Z. Jang, *Nano Letters* **10**, 4863 (2010).

[15] Z. Wu, E.Wang, G. Zhang, Y.Shen, G.Shao, *Small* **20**, 2307923 (2024).

[16] D. H. Seo, Z. J. Han, S. Kumar, and K. Ostrikov, *Advanced Energy Materials* **3**, 1316 (2013).

[17] H. Yang, J. Yang, Z. Bo, S. Zhang, J. Yan, K. Cen, Journal of Power Sources **324,** 309 (2016).

[18] S. R. Polaki, N. G. Krishna, M. Kamruddin, and K. Ostrikov, Energy Storage Materials **16**, 150 (2019).

[19] D. H. Seo, S. Pineda, J. Fang, Y. Gozukara, S. Yick, A. Bendavid, S. H. Lam, A. T. Murdock, A. B. Murphy, Z. J. Han, and K. Ostrikov, ACS Sustainable Chemistry & Engineering, **3**, 544 (2015).

[20] S. Sahoo, G. Sahoo, S. M. Jeong, Journal of Energy Storage **53**, 105212, (2022).

[21] Z. Bo, S. Mao, Z. J. Han, K. Cen, J. Chen, and K. Ostrikov, *Chem. Soc. Rev.* **44**, 2108 (2015).

[22] S. Ghosh, S. R. Polaki, N. Kumar, S. Amirthapandian, M. Kamruddin, K. Ostrikov, Beilstein Journal of Nanotechnology **8**, 1658 (2017).

[23] T.-T. Zhang, B.-H. Lv, C.-C. Fan, B.-Y.Shi**,** Q.-J. Cao, W. Wang**,** F.-F. Tao, W.-D. Dou, ACS Omega **8**, 36245 (2023).

[24] S. Xie, J. Huang, Y. Zhang, W. Cai, and X. Zhang, *Nanomaterials*, *11*, 1268. (2021).

[25] M. Cai, R. A. Outlaw, R. A. Quinlan, D. Premathilake, S. M. Butler, and J. R. Miller, ACS Nano **8**, 5873 (2014).

[26] P. Ji, J. Chen, T. Huang, C. Jin, L.Zhuge, X.Wu, Diamond and Rel.Mat. **108,** 107958 (2020).

[27] J.-Y.Tung, K.-P.Huang , Journal of the Taiwan Institute of Chemical Engineers **163**, 105663, (2024).

[28] H. Mehdipour and K. Ostrikov, ACS Nano 6, 10276 (2012).

[29] Z. Bo, S. Mao, Z. J. Han, K. Cen, J. Chen, K. Ostrikov, Chem. Soc. Rev. **44**, 2108 (2015).

[30] S. Ghosh, S. R. Polaki, N. Kumar, S. Amirthapandian, M. Kamruddin, K. Ostrikov, Beilstein J Nanotechnol **8**, (2017).

[31] P. R. Bandaru, H. Yamada, R. Narayanan and M. Hoefer, Nanotechnol Rev 6, 421 (2017).

[32] B.E. Conway, Electrochemical Supercapacitors: Scientific Fundamentals and Technological Applications. Springer (1999).

[33] P. Simon and Y. Gogotsi, Nature Materials **7**, 845 (2008).

[34] S. Ghosh, T. Mathews, B. Gupta, A. Das, N. G. Krishna, M. Kamruddin, Nano Structures & Nano-Objects **10**, 42 (2017).

[35] J. L. Qi, X. Wang, J. H. Lin, F. Zhang, J. C. Feng and W.-D. Fe, Nanoscale **7**, 3675 (2015).

[36] N.Gupta, R. Gupta, S.C.Sharma, Contrib. Plasma Phys.**61**, e202100069 (2021).

[37] M. A. Lieberman and A. J. Lichtenberg, Principles of Plasma Discharges and Materials Processing (2nd ed.). John Wiley & Sons (2005).

[38] I. B. Denysenko, S. Xu, J. D. Long, P. P. Rutkevych, N. A. Azarenkov, K. Ostrikov, J. Appl. Phys. **95**, 2713 (2004).

[39] H. Mehdipour and K. Ostrikov, ACS Nano 6, 10276 (2012).

[40] H.O. Pierson, Handbook of Carbon, Graphite, Diamond and Fullerenes: Processing, Properties and Applications, Noyes Publications, New Jersey (1993).

[41] D.D.L. Chung, Review: Graphite, Journal of Materials Science **37** 1475 (2002).

[42] Hamid Mehdipour and Kostya (Ken) Ostrikov, *ACS Nano*, 6(11), 10276 (2012).

[43] M. C. Stoian, O. G. Simionescu, C. Romanitan, G. Craciun, C. Pachiu and A. Radoi, Sensors **24**, 7194 (2024).

[44] N. Namdar, F.Ghasemi, and Z. Sanaee, Scientific Reports **12**, 4254 (2022).

[45] I. B. Denysenko, K. Ostrikov, M. Y. Yu, and N. A. Azarenkov, J. Appl. Phys. **102**, 074308 (2007).

[46] K. Ostrikov, E. C. Neyts & M. Meyyappan, Advances in Physics, 62(2), 113 (2013).

[47] R. Narayanan, H. Yamada, M. Karakaya, R. Podila, A. M. Rao, P. R. Bandaru, Nano Lett. **15**, 3067(2015).

[48] S. Ghosh, S. R. Polaki, M. Kamruddin, S. M. Jeong and K. Ostrikov, Journal of Physics D: Applied Physics **51**, 145303 (2018).

[49] M. Hiramatsu, M. Hori, Carbon Nanowalls: Synthesis and Emerging Applications, Springer (2010).

[50] H. J. Cho, H. Kondo, K. Ishikawa, M. Sekine, M. Hiramatsu, M. Hori , Carbon **68**, 380 (2014).

[51] S. Ghosh, T. Mathews, B. Gupta, A. Das, N. G. Krishna, M. Kamruddin, Nano-Structures & Nano-Objects **10**, 42 (2017).

[52] G. Sahoo, S. R. Polaki, S. Ghosh, N. G. Krishna, and M. Kamruddin, Journal of Power Sources **401**, 37(2018)).

[53] M. Mao, A.Bogaerts, J. Phys. D: Appl. Phys. **43**, 205201 (2010).

[54] H. J. Cho, H. Kondo, K. Ishikawa, M. Sekine, M. Hiramatsu, M. Hori, Carbon **68**, 380 (2014).

[55] Y. Ma, W. Jiang, J. Han, Z. Tong, M. Wang, J. Suhr, X. Chen, L. Xiao, S. Jia, H. Chae, ACS Appl. Mater. Interfaces **11**, 10237 (2019).

[56] A. Jafari, M. Ghoranneviss, M. R. Hantehzadeh, A. Boochani, J. Chem. Res. **40**, 40 (2016).

[57] W. Z. Collison, T. Q. Ni, M. S. Barnes, J. Vac. Sci. Technol. A **16**, 100 (1998).

[58] W. Takeuchi, H. Sasaki, S. Kato, S. Takashima, M. Hiramatsu, M. Hori, J. Appl. Phys. **105**, 113305 (2009).

[59] J. R. Miller, R. A. Outlaw, and B. C. Holloway, Science **329**, 1637 (2010).